

## Wavelet Analysis of Geophysical Well-log Data of Bombay Offshore Basin, India

E. Chandrasekhar · V. Eswara Rao

Received: 3 February 2012 / Accepted: 11 September 2012 / Published online: 13 October 2012  
© International Association for Mathematical Geosciences 2012

**Abstract** Geophysical well-log (bore-hole) data facilitate understanding of the physical properties of the subsurface formations as a function of depth measured in a well. In the present study, the wavelet transformation technique was applied to the well-log data of three wells in the Bombay High oil field, India, in order to identify depths to the tops of oil and/or gas formation zones (pay zones). Continuous wavelet transformation (CWT) was performed on gamma-ray, resistivity, neutron porosity and velocity log data sets in order to determine the space-localization of the oil and/or gas formation zones. The choice of a mother wavelet is important and largely depends on the data under investigation. We have applied a variety of wavelets to the different log data sets to not only identify the depths to the tops of formation zones, but also to determine the optimum wavelet that best characterizes the pay zones. On examination of scalogram plots of each log corresponding to each wavelet for their better resolution in identifying the formation boundaries, we have found that the scalograms corresponding to the Gaus1 wavelet appeared to give the best resolution in identifying the depths of pay zones in all the well-log data sets of all three wells. To further validate the above observation, a histogram analysis of CWT coefficients is made. This showed that, of all the wavelets considered for the present study, Gaus1 wavelet is the most appropriate and optimum for determining the space-localization of pay zones in all the well-log data sets considered in the present study. The depths of pay zones estimated from scalogram plots of logs agree well with those provided by the Oil and Natural Gas Corporation Ltd., India.

**Keywords** Well-log data · Continuous wavelet transformation · Bombay offshore basin, India

---

E. Chandrasekhar (✉) · V. Eswara Rao  
Department of Earth Sciences, Indian Institute of Technology Bombay, Powai, Mumbai 400076,  
India  
e-mail: [esekhar@iitb.ac.in](mailto:esekhar@iitb.ac.in)

## 1 Introduction

Most previous well-log data analyses involved direct interpretation of data using visual inspection and comparison between different logs. However, in the past three decades, efforts to improve mathematical and data processing techniques have been steadily progressing for improved understanding and interpretation of well-log data, particularly for sedimentological and stratigraphic studies. Using the concept of electrofacies (a set of log responses which characterizes a bed and distinguishes it from others) introduced by Serra and Abbot (1982), Wolff and Pelissier-Combesure (1982) developed an algorithm based on Principal Component Analysis for automatic detection of electrofacies. Anxiennaz et al. (1990) carried out cluster analysis for identification of lithofacies. Other methods include Fourier transformation studies (Tiwari 1987) and semivariogram analysis (Jennings et al. 2000) to study periodicities and assess the degree of similarity between sample pairs as a function of separation distance within the subsurface formations.

Since different subsurface formations have various physical properties, which in turn reflect different frequency characteristics, understanding their frequency characteristics vis-à-vis their spatial location is always important and useful. However, the conventional signal processing techniques can only tell whether or not some particular frequencies (representative of formations) of interest are present in the signal, and thus they fail to explain which frequencies (formations) occur at what depths. This is known as space-frequency localization. Therefore, effective signal processing tools that can provide information about the space-localization of the formations is required. Wavelet analysis has been one of the most efficient mathematical tools for facilitating a comprehensive understanding of composite signals like well-logs. Wavelet analysis of logs can identify cyclicities and depth locations of formation tops, thus providing space localizations of different formations. Wavelet analyses have been applied for many purposes. This includes hydrocarbon production data for estimating the preferential flow paths and the existence of flow barriers within the reservoir rocks (Jansen and Kelkar 1997), determining high frequency sedimentary cycles of oil source rocks (Prokoph and Agterberg 2000), identifying reservoir anomalies from pressure transient data (Panda et al. 2000; Soliman et al. 2001), as well as for feature extraction in well-log data (Rivera et al. 2002, 2004) and gamma-ray log data to identify depths to the tops of the formation zones (Choudhury et al. 2007). Vega (2003) used pattern recognition technique and identified the formation tops and discontinuities present in each well and studied well-to-well stratigraphic correlation. All these techniques have been proved to be helpful for better understanding of subsurface layers, compared to the conventional correlations using visual inspection of well-logs.

In the present study, we have analyzed different well-log data sets recorded at three wells in the Bombay offshore basin in western India, using continuous wavelet transformation (CWT) to provide space localization of the pay zones. We have examined a variety of wavelets to identify suitable wavelet(s) that can best resolve the space localization of the formation zones. We further have extended our search to find an optimum wavelet that best suits well-log data by analyzing the histograms of CWT coefficients. The organization of this paper is as follows. Section 2 summarizes the

**Fig. 1** Geographical location of the Bombay High and its contiguous regions in Western India. The data for the present study has been procured from this region (redrawn from database supplied by ONGC Ltd.)



geology and lithostratigraphy of the study area. Section 3 details the data used. Section 4 describes the wavelet analysis of well-log data, and Sect. 5 provides the details of analysis results and discussion.

## 2 Geology and Lithostratigraphy of the Study Area

Bombay High is the largest hydrocarbon field in India belonging to the western offshore basin (Fig. 1). The main oil and gas reserves (pay zones) are L-I, L-II, L-III (limestone) and S-I (sandstone), located in the cenozoic sedimentary succession, which rests either on the Cretaceous Deccan basalt or Archean metamorphic basement (Bhandari and Jain 1984). Of these, the L-III is the largest and the most productive of all the pay zones. Figure 2 summarizes the stratigraphy, lithological variations, seismic markers, and pay horizons of the Bombay High field. More geological and lithostratigraphic details of the field can be found in Rao and Srivastava (1981), Biswas (1982), and Bhandari and Jain (1984).

## 3 Data Base

For the present study, gamma-ray, resistivity, neutron porosity, and velocity ( $V_p$ ) well-log data sets from three vertical wells, viz. Well-A, Well-B, and Well-C have been procured from the Oil and Natural Gas Corporation (ONGC) Limited, India. The wells, located in the Bombay High oilfield in the western offshore basin (Fig. 1) are separated by a distance of approximately 10 km. Logs of all three wells represent subsurface sections of approximately 500 m below the sea floor. The original data, available in DLIS (Digital Log Interchange Standard) format were converted

into ASCII, before further processing. Velocity log data (in units of m/s) were generated from the sonic log. Data were sampled at 0.15 m and a total of 3280 data points in each log of all three wells were obtained. Figure 3 depicts different log data sets as a function of depth (with depth scale increasing from top [sea floor] to bottom), corresponding to Well-A (Fig. 3a), Well-B (Fig. 3b), and Well-C (Fig. 3c).

Age	Average thickness (m)	Lithology	Seismic Marker	
Holocene to Pliocene	600	Clay and claystone	—	—
		unconformity	—	—
Late Miocene	250	Thick shale with minor limestone	—	—
		unconformity	—	—
Middle Miocene	70	Limestone with minor shale	L-I	Horizon-I
		unconformity	L-II	
		Shale with prominent fine sandstone, siltstone bands in the middle	S-I	—
	300	unconformity	—	—
Early Miocene	470	Thick limestone with thin dark grey and green shale	L-III	Horizon-II
Late Oligocene	100	Limestone/shale alteration	L-V	—
		unconformity	—	—
Paleocene	10	Trap wash	—	—
		non-conformity	—	—
		Basalt / Archean Metamorphics	—	—

Fig. 2 Lithostratigraphic details and seismic marker locations of Bombay High field (not to scale, after Bhandari and Jain 1984)

Fig. 3 Gamma-ray log, resistivity log, neutron porosity log and velocity log data corresponding to Well-A (a), Well-B (b), and Well-C (c) from the Bombay offshore basin, India

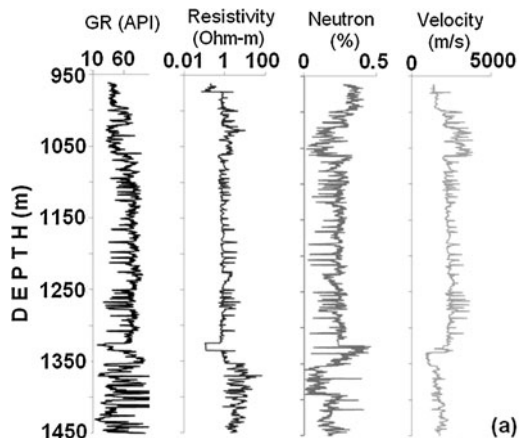
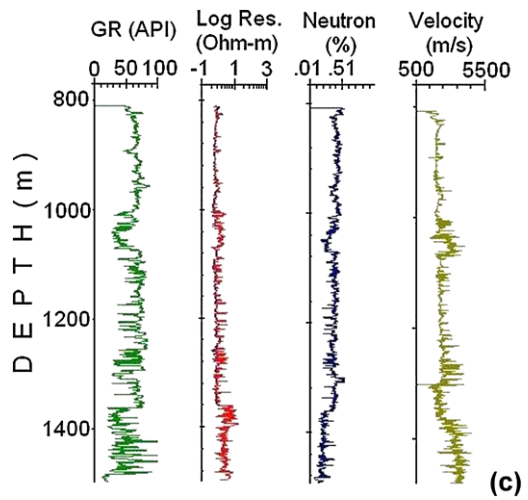
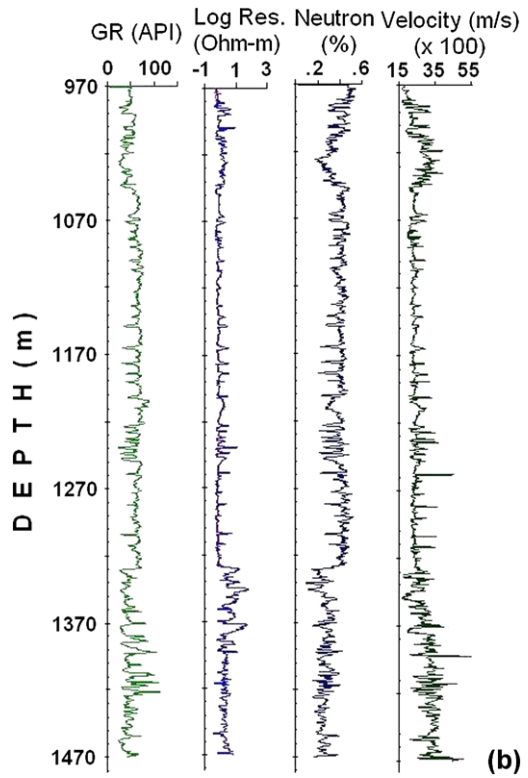
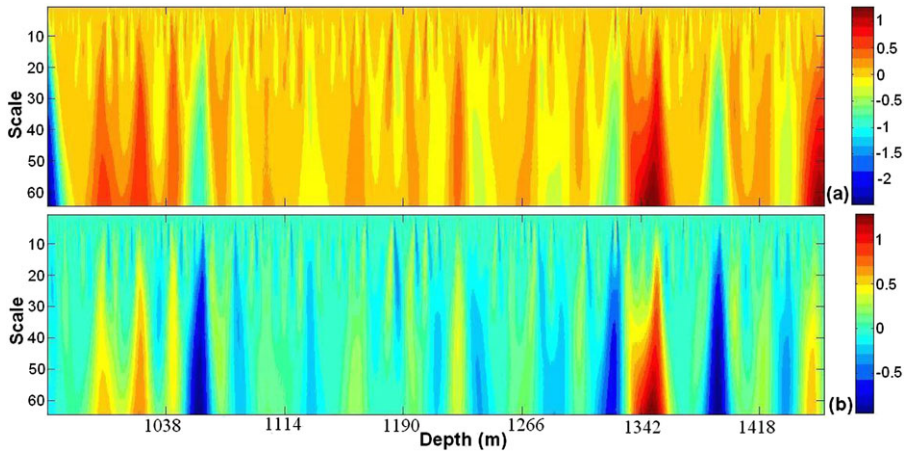


Fig. 3 (Continued)





**Fig. 4** Example of scalogram plots of CWT analysis of neutron porosity log data of Well-A, when edge effects in the signal are not removed (a) and removed (b). Note the high resolution of marker horizons in (b) than in (a)

## 4 Wavelet Analysis

### 4.1 Theory

The wavelet function,  $W_{d,s}(x)$ , signifying the frequency-space localization is defined as

$$W_{d,s}(x) = \frac{1}{\sqrt{s}} \psi \left( \frac{x-d}{s} \right), \quad (1)$$

where  $s > 0$  indicates the scale and  $d$  indicates the shift parameter.  $s$  is analogous to frequency, in the sense that the higher scales provide details of long-wavelength features of the signal and the lower scales provide details of the short-wavelength features of the signal.  $d$  refers to depth information in the transformed domain in this application. The function  $W_{d,s}(x)$  is called analyzing wavelet or mother wavelet. More details about the fundamentals of wavelet theory can be found in Daubechies (1992), Mallat (1989, 1999), and references therein.

In wavelet transformation, the signal to be transformed is convolved with the mother wavelet and the transformation is computed for different segments of the data by varying  $d$  and  $s$ . The wavelet transformation in which the shifts and dilations will be continuously varied is called CWT and the transformation in which they will be varied as power of an integer  $n$  (that is:  $n^j$ ,  $j = 1, 2, 3, \dots, k$ ) is called Discrete Wavelet Transformation (DWT) (Ma and Tang 2001). Generally in DWT, dyadic scales and shifts are used, in which case  $n = 2$ . Although both CWT and DWT are linearly shift-invariant, the difference between them is as follows. In case of CWT, an amount of small spatial shift ( $\delta d$ ) in the wavelet function results in the same amount of shift in the transformed domain. As a result, abrupt changes (spikes, etc.) in the data can be effectively picked up by performing the computations at chosen variations in shifts. On the other hand, in case of DWT, the wavelet transform

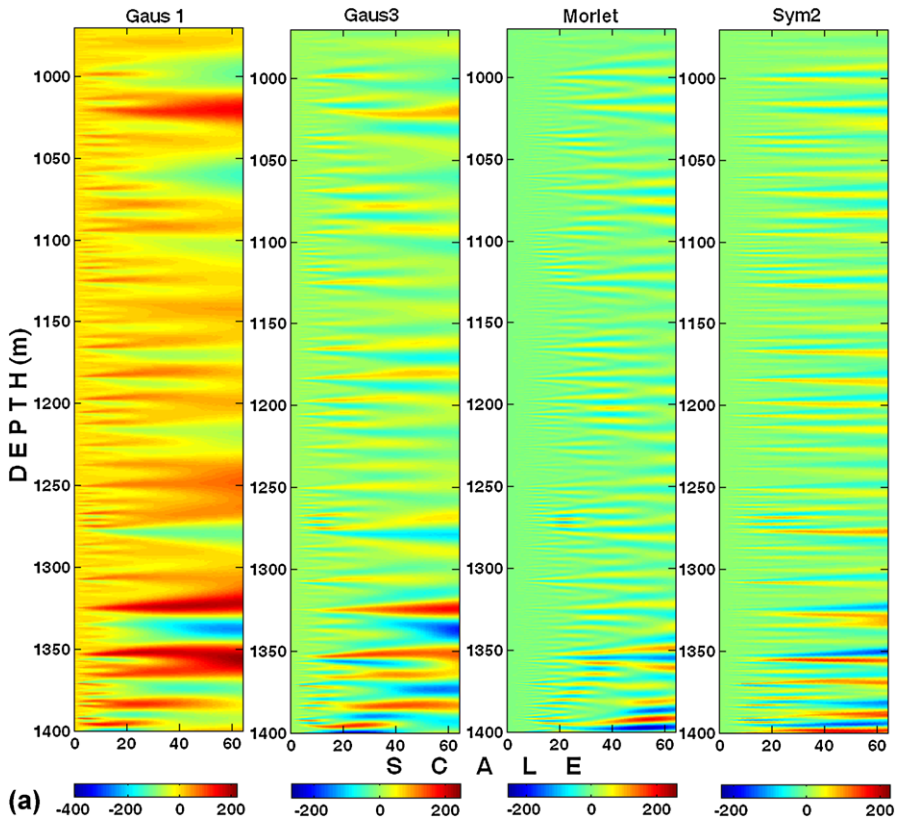


**Fig. 5** Scalogram plots of log data of Well-A when Gaus1, Gaus3, Morlet, and Sym2 wavelets were applied to (a) gamma-ray log, (b) resistivity log, (c) neutron porosity, and (d) velocity logs

coefficients become shift invariant only if the shifts are in dyadic steps (that is, as a power of 2) (Ma and Tang 2001). Therefore, if DWT is applied to well-log data, there may arise a possibility that the identification of location of some peaks associated with the frequencies of interest are missed in such dyadic steps of shifts. Therefore, DWT is not suitable for the present study. Mathematical details of the shift-invariant property of wavelets is given in Appendix A.

CWT, defined as the inner product of the mother wavelet  $W_{d,s}(x)$  (Eq. (1)) and the signal,  $f(x)$ , is given by

$$CWT_x(d, s) = \frac{1}{\sqrt{s}} \int_{-\infty}^{\infty} f(x) \psi\left(\frac{x-d}{s}\right) dx. \tag{2}$$

CWT coefficients are estimated at each  $s$  by continuously varying  $d$ . The larger the value of the CWT coefficient, the greater the similarity between the shapes of the signal and the wavelet at  $d$  and  $s$ , signifying the suitability of the chosen mother

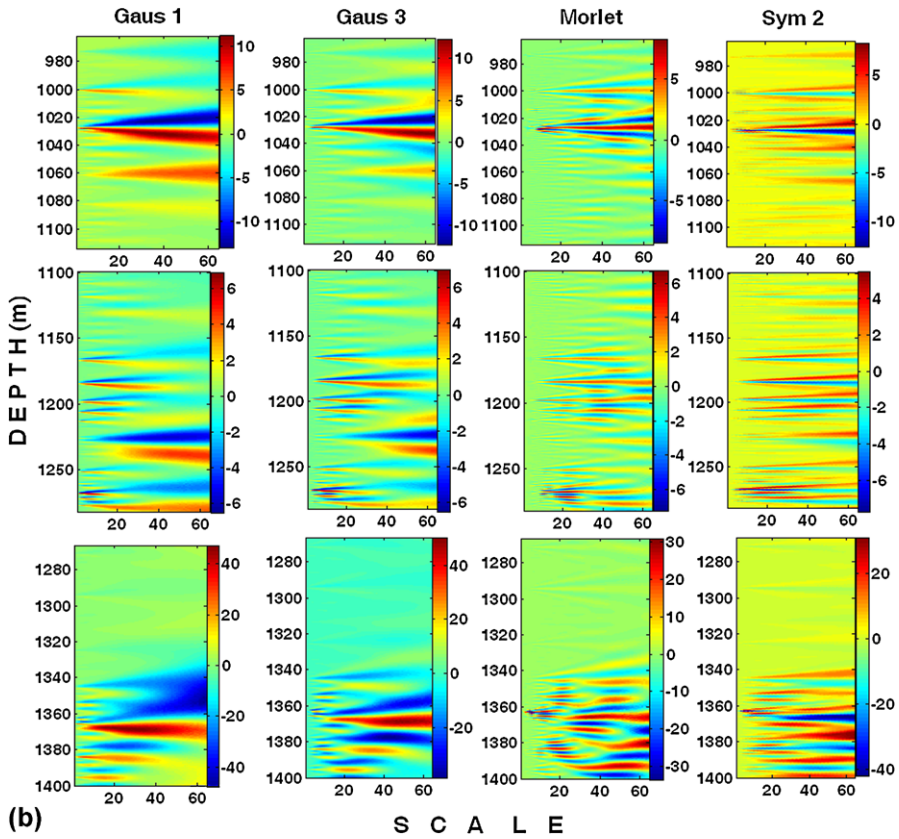


Fig. 5 (Continued)

wavelet for analyzing the signal. CWT was performed on the fully processed data using a variety of wavelets.

### 4.2 Continuous Wavelet Transformation

CWT was performed on different well-log data sets, viz. the gamma-ray log, resistivity log, neutron log and velocity log of three wells: Well-A, Well-B, and Well-C. A variety of wavelets was used in order to select the optimum one(s). On examination of the scalograms (contour plots of absolute CWT coefficients) of each log corresponding to each wavelet, we first have found that the edge effects in the signal have resulted in producing high values of CWT coefficients at the ends of scalograms, which have masked the features of subsurface formations of interest in the data. Therefore, prior to further analysis, the edge effects were removed from the data using the symmetric half-point method (Strang and Nguyen 1995). Figure 4



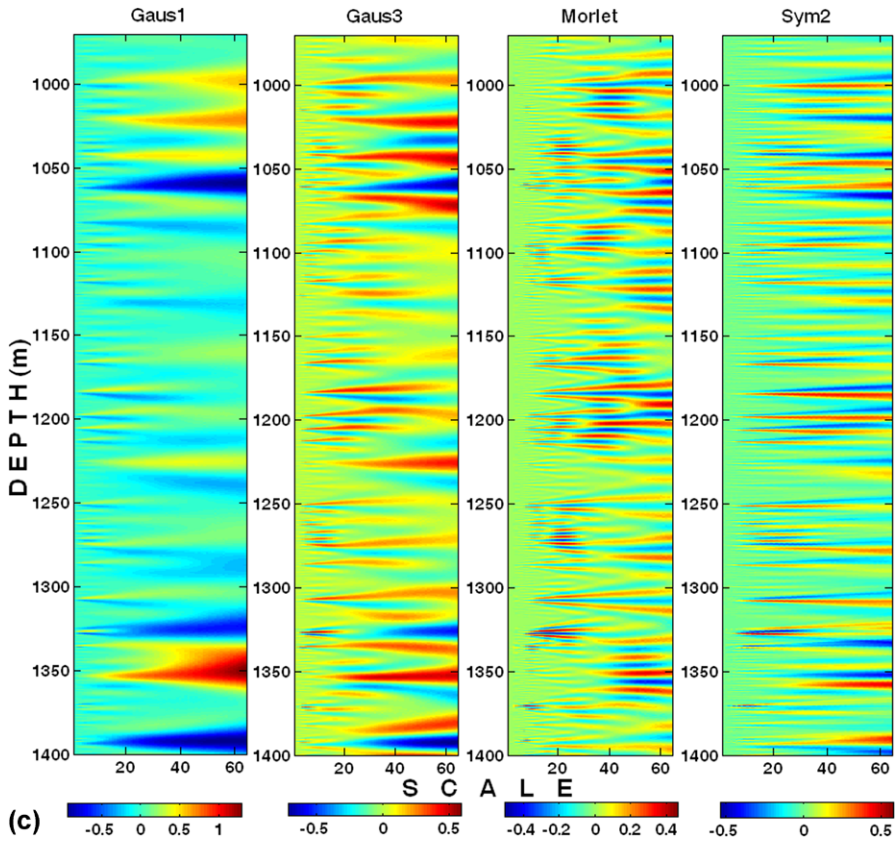
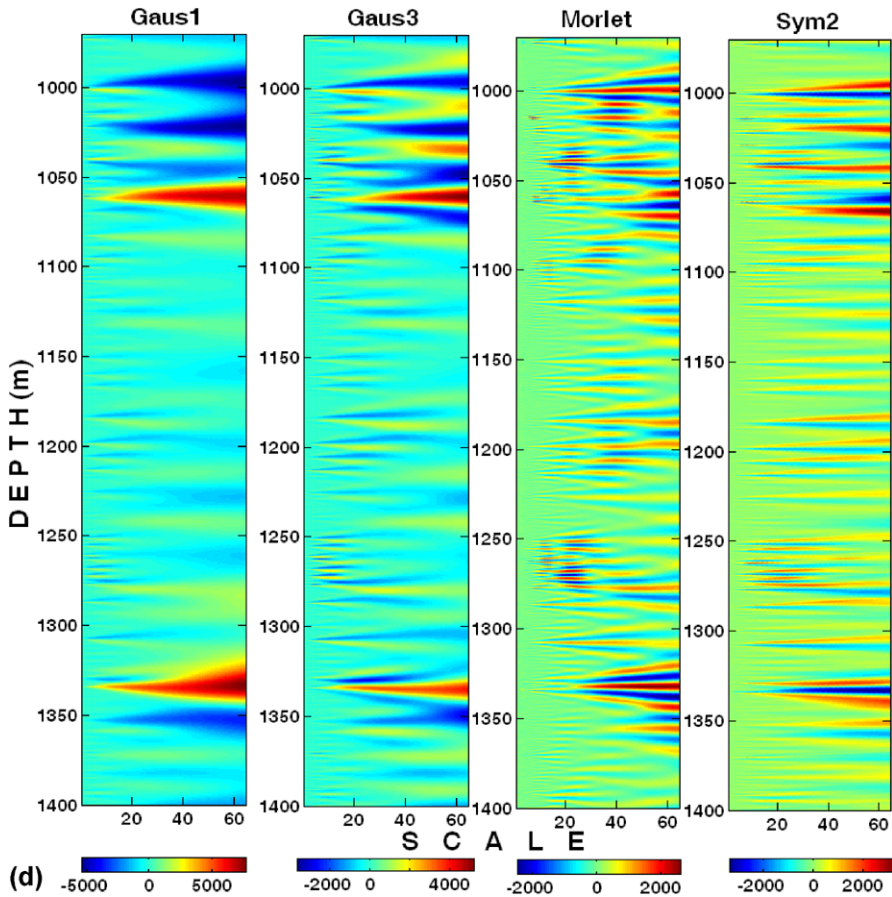


Fig. 5 (Continued)

shows an example of the scalogram of the neutron porosity log of Well-A obtained with Gaus1 wavelet, before (Fig. 4a) and after (Fig. 4b) removing edge effects. The resolution of the subsurface features is more apparent in Fig. 4b than in Fig. 4a. Cosine tapering is another method generally used to remove the edge effects in the signal.

On observation of the obtained CWT results of several wavelets, we have found that three wavelets viz. Gaus1, Gaus3, and Sym2 wavelets have shown acceptable resolution in identifying the formation boundaries in the scalogram plots. We also have used the Morlet wavelet as it was found to be an optimum one for boundary detection and cyclostratigraphic studies of well-log data by Vega (2003) and for Gamma-ray log data analysis by Choudhury et al. (2007). The shapes of Gaus1, Gaus3, Morlet, and Sym2 wavelets together with their properties are given in Appendix B. Figure 5 shows the scalograms corresponding to Gaus1, Gaus3, Morlet, and Sym2 wavelets of gamma-ray log (Fig. 5a), resistivity log (Fig. 5b), neutron porosity log (Fig. 5c) and velocity log (Fig. 5d) of Well-A. Similarly, Figs. 6 and 7 show the scalogram plots corresponding to Gaus1, Gaus3, Morlet, and Sym2 wavelets of the gamma-ray log



**Fig. 5** (Continued)

(Figs. 6a, 7a), resistivity log (Figs. 6b, 7b), neutron porosity log (Figs. 6c, 7c) and velocity log (Figs. 6d, 7d) of Well-B and Well-C, respectively.

### 4.3 Histogram Analysis

Histogram plots between the CWT coefficient values and the maximum number of times each coefficient occurs in the CWT analysis of the entire signal were generated corresponding to each wavelet and each log of all three wells. They are shown in Fig. 8a (Well-A), Fig. 8b (Well-B), and Fig. 8c (Well-C). The number of occurrences designates the number of times a CWT coefficient occurred. That means, for example, in Fig. 8a the CWT coefficient values ranging from 100–125 and 125–150 occur about 125 and 100 times, respectively, in the analysis of the gamma-ray log data using the Gaus1 wavelet for Well-A. This implies that the suitability of a wavelet for analyzing a signal becomes important, only when the number of occurrences of high CWT coefficients is more for that wavelet.

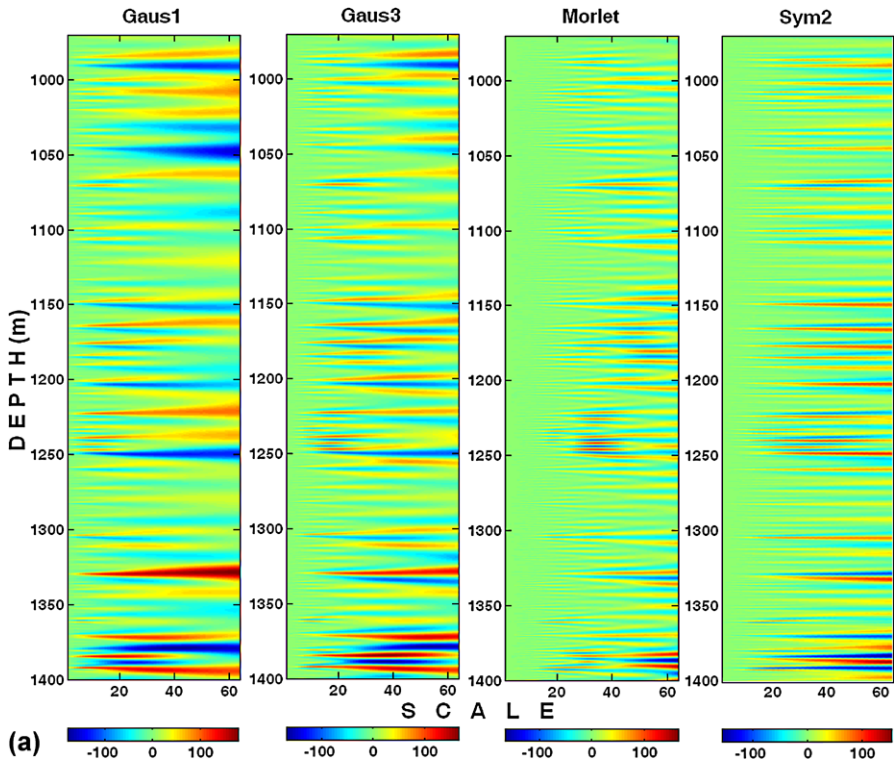


**Fig. 6** Scalogram plots of log data of Well-B when Gaus1, Gaus3, Morlet and Sym2 wavelets were applied to (a) gamma-ray log, (b) resistivity log, (c) neutron porosity, and (d) velocity logs

### 5 Results and Discussion

Shale (sand) formations show high (low) gamma-ray intensity. Since we are interested in identifying reservoir rocks (which are nonshaly), identification of boundaries between different subsurface formations in well-log data becomes necessary. A careful examination of scalograms corresponding to the gamma-ray logs of Well-A (Fig. 5a), Well-B (Fig. 6a), and Well-C (Fig. 7a) clearly shows that among the four wavelets, the results of Gaus1 wavelet reveal a clear shale/sand transition zone with well marked high (red) and low (blue) CWT coefficients, clearly delineating the boundaries between the shaly and sandy formations as a function of depth. This indicates that the Gaus1 wavelet is more suitable at effectively resolving the marker horizons in the gamma-ray log data (Fig. 8). For the gamma-ray log data, although such a resolution is less distinct in the scalogram of Gaus3 wavelet compared to that of Gaus1, the resolution is even lower in the scalograms of Morlet and Sym2 wavelets. The poor resolution in the latter case could be due to the mismatch between the shapes of Morlet and Sym2 wavelets and the signal, at different shifts and dilations. As a result, the continuous shifts and dilations of these wavelets in CWT operation on the gamma-ray log data might have averaged out the CWT coefficients at depths of L-I, L-II, S-I, and L-III formations, leading to smeared resolution about

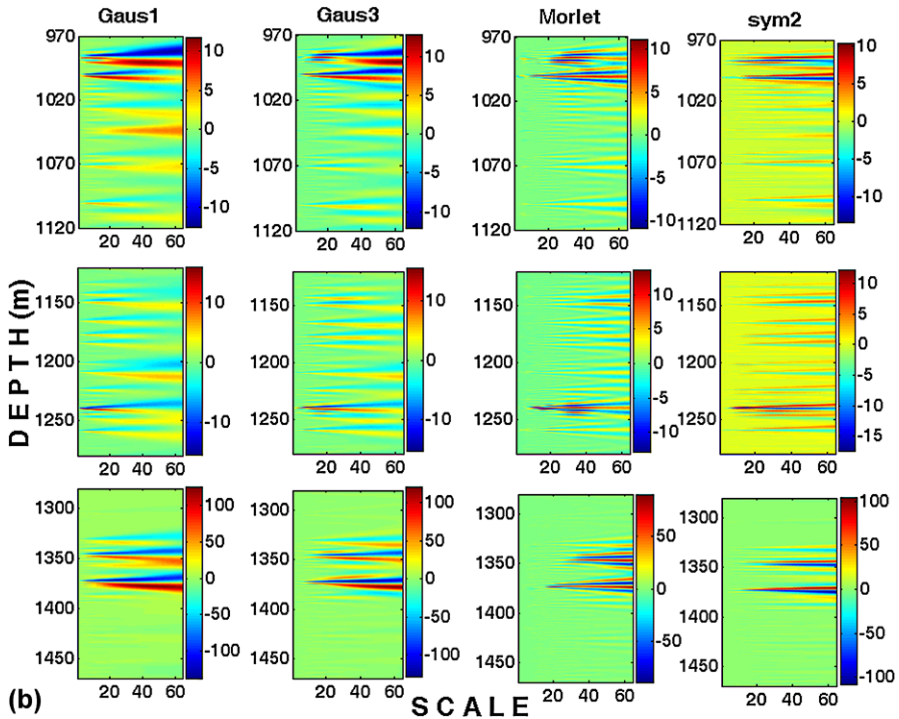


**Fig. 6** (Continued)

the depth locations of the above formations. The estimates of the depths to the tops of the L-I, L-II, S-I, and L-III formations obtained from the scalogram plots of all the wavelets corresponding to all the wells are given in Tables 1, 2, 3, 4. The known depth estimates of these formations in the study area, provided by ONGC Ltd. are also given in Tables 1, 2, 3, 4. ONGC Ltd. has estimated these values using conventional well-log data analysis and the core samples.

The scalograms associated with resistivity data are shown in three parts for each well (Figs. 5b, 6b, and 7b). When the entire resistivity log data were considered as a single trace and analyzed, the very high resistivity of the thick pay zone, L-III, has masked the resolution of the formation tops of L-I, L-II, and S-I formations, and thus it became difficult to identify the correct depth estimates of these formations. This has been the case with the resistivity log data of the other two wells as well. Therefore, the data of each well were first divided into three parts with overlapping data levels with each part individually analyzed. Resistivity of the reservoir rock mainly depends on the resistivity of the fluid (water/oil) present in it. Hydrocarbon-bearing formations are characterized with high resistivity compared to those of non-hydrocarbon-bearing formations. Accordingly, scalograms of the resistivity logs of Well-A (Fig. 5b), Well-B (Fig. 6b), and Well-C (Fig. 7b) show clear distinction between the alternating

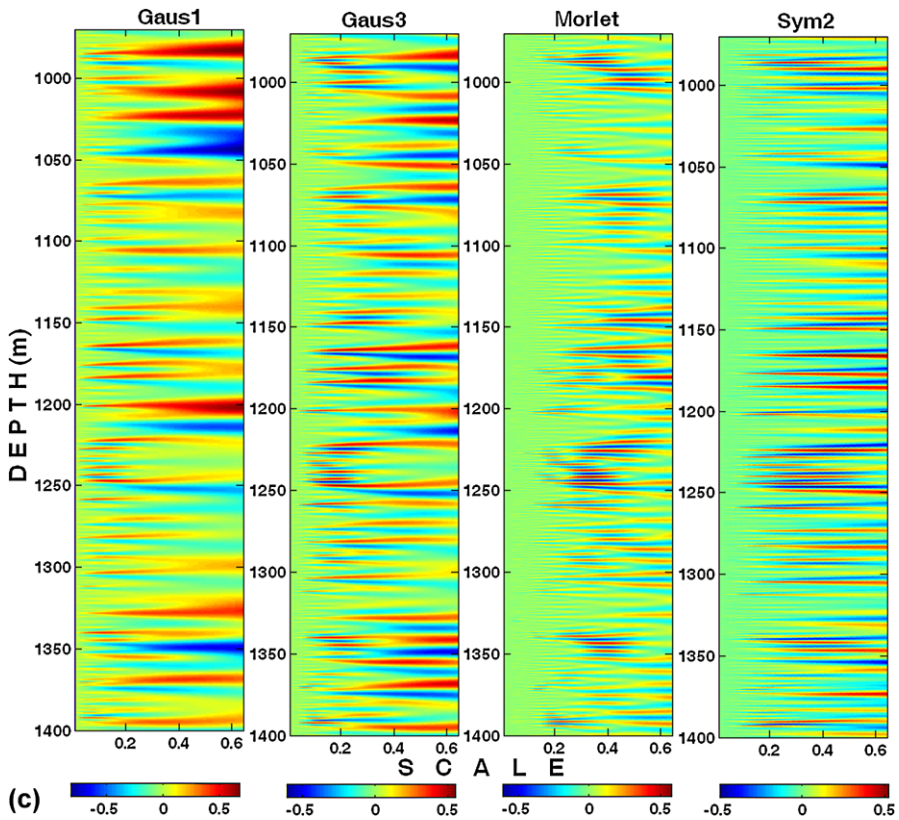


**Fig. 6** (Continued)

sequences of such formations in all three wells. The four formation tops L-I, L-II, S-I, and L-III could be clearly identified in the scalograms of the Gaus1 and Gaus3 wavelets, showing considerable resolution in delineating these formation tops. Although Morlet and Sym2 wavelets show some acceptable resolution in identifying the depths to tops of the above formations corresponding to resistivity data, the depth resolution of S-I in Well-A and L-II and S-I in Well-B, particularly due to Morlet wavelet is very poor (Tables 3 and 4).

Study of the scalograms of the neutron porosity logs of Well-A (Fig. 5c), Well-B (Fig. 6c), and Well-C (Fig. 7c) show high positive coefficients at different depths corresponding to the decrease in neutron porosity. Generally, shaly formations show higher neutron porosity than the nonshaly formations because of the clay bound water. Hence, a decrease in neutron porosity is an indication of change of nonreservoir rock to reservoir rock. Here again, the clear transition between the positive and negative CWT coefficients, representative of clear demarcation between reservoir and nonreservoir rocks, is conspicuous in the scalogram plots of Gaus1 wavelet for all the three wells. The depth estimates derived from the scalogram plot of Gaus1 wavelet corresponding to these four formation tops L-I, L-II, S-I, and L-III of all the wells also match well with those of the known estimates provided by ONGC Ltd. (Table 1).

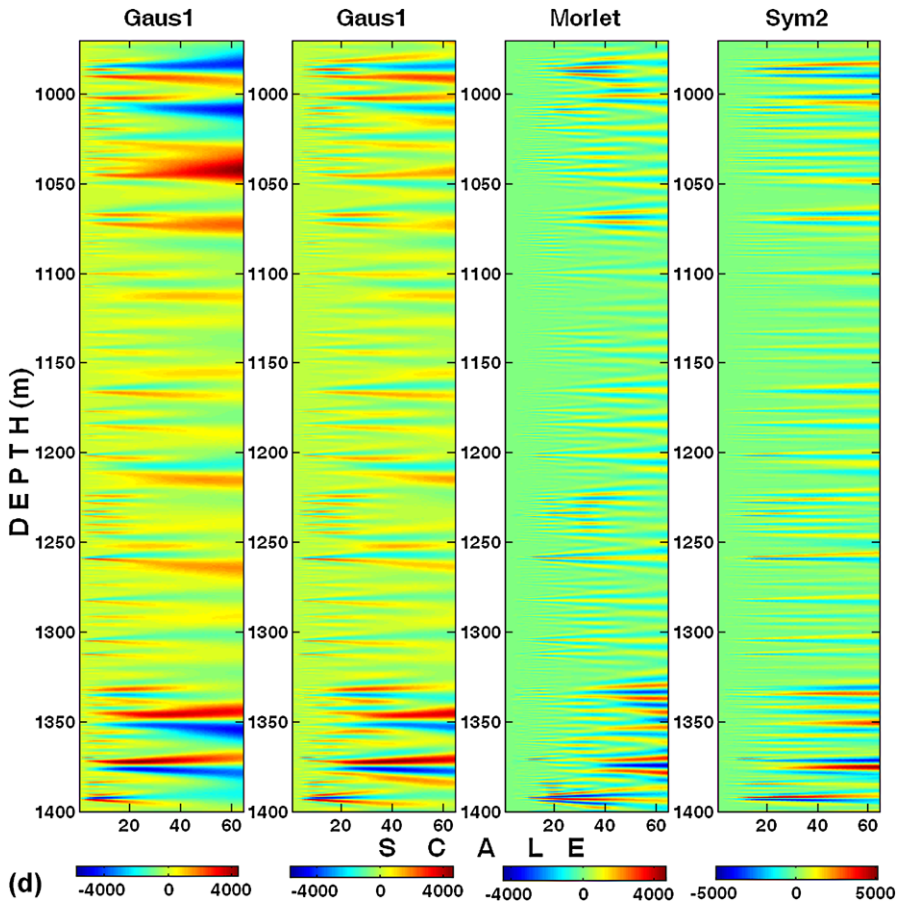


**Fig. 6** (Continued)

Although Gaus3 wavelet also gives an acceptable resolution, the histogram analysis clearly suggests that Gaus1 wavelet is superior to the Gaus3 wavelet (Fig. 8). The depth resolution of the L-I, L-II, and S-I formation tops is again poor in the scalogram plots of Morlet and Sym2 wavelets, corresponding to neutron porosity log data (Figs. 5c, 6c, and 7c).

Velocity logs generated from sonic logs measure the interval transit time of sound waves in the formations. As expected, velocities are usually low for the reservoir rocks (lime stone and sand stone) when compared to shaly formations. Accordingly, the scalograms of the velocity logs of Well-A (Fig. 5d), Well-B (Fig. 6d), and Well-C (Fig. 7d), clearly show the marked distinction between sand and shaly formations representative of different velocities. Among the four wavelets used in the analysis, scalograms of Gaus1 wavelet show clear resolution in identifying the space localization of the four formation tops L-I, L-II, S-I, and L-III (Table 2). Figures 5d, 6d, and 7d, and also Tables 3 and 4 clearly show that identifying the depth locations of the above four formations zones is very difficult with Morlet and Sym2 wavelets.

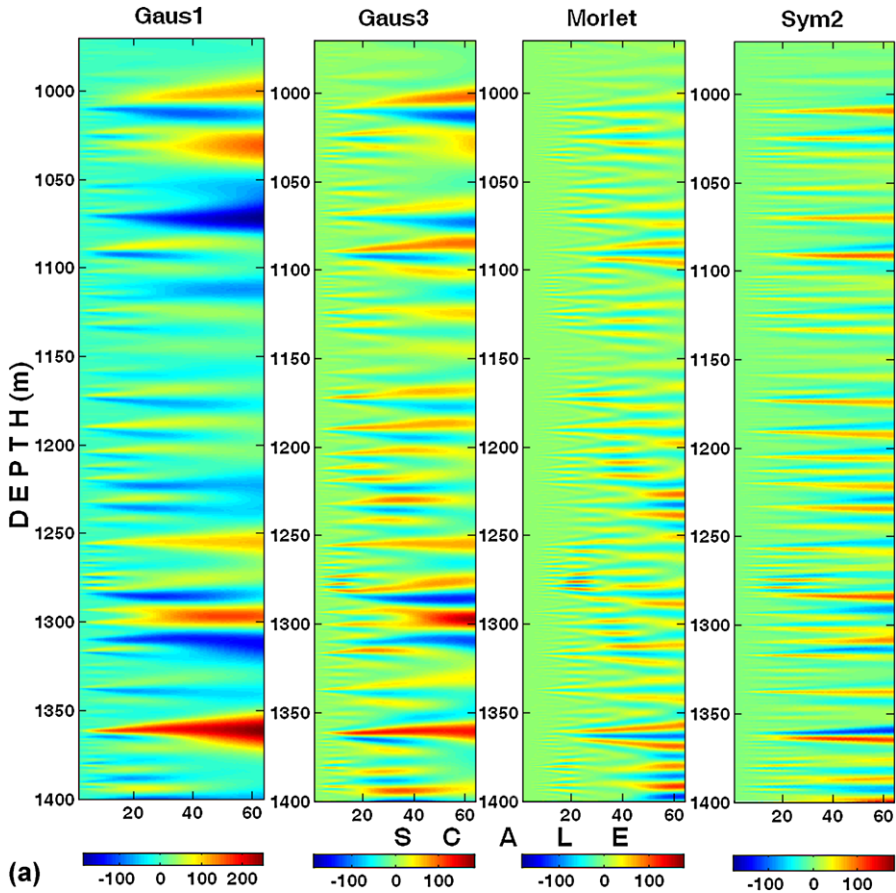


**Fig. 7** Scalogram plots of log data of Well-C when Gaus1, Gaus3, Morlet, and Sym2 wavelets were applied to (a) gamma-ray log, (b) resistivity log, (c) neutron porosity, and (d) velocity logs

A careful observation of the histogram plots shown in Fig. 8 suggests that the Gaus1 wavelet appears to be the most suitable wavelet for analysis of well-log data of all three wells, because the number of occurrences of high CWT coefficients is more for the Gaus1 wavelet than any other wavelet. This in turn explains the suitable match between the shape of the Gaus1 wavelet and the well-log data. It is pertinent to mention here that the shape of the Gaus1 wavelet (see Appendix B), which shows a positive peak followed by a negative peak, matches well with the signatures of alternate sequences of shale and sand formations during the CWT operation, when the wavelet is shifted and dilated. Accordingly, this results in producing high CWT coefficients for all log-data sets with Gaus1 wavelet. Interestingly, it can also be shown mathematically that Gaussian functions will have the least uncertainty in effective representation of signals in a time-frequency frame. Appendix C provides a brief mathematical description of the same. However, compared to those of the Gaus1 and Gaus3 wavelets, the number of occurrences of high CWT coefficients of Morlet and Sym2 wavelets is very few corresponding to all the well-logs of all three wells

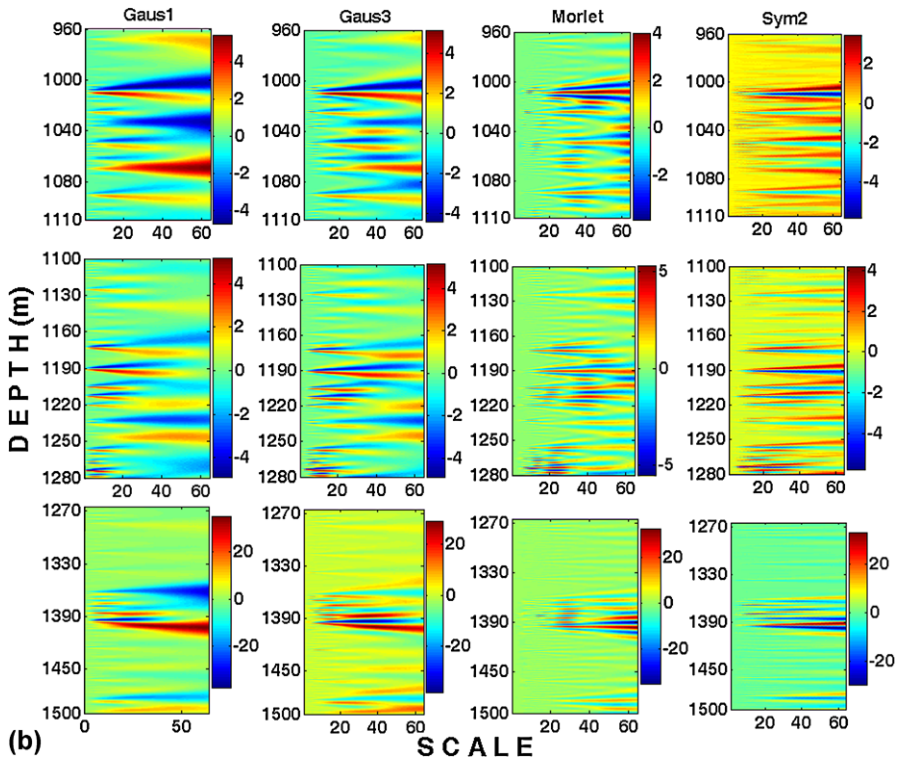


**Fig. 7** (Continued)

(Fig. 8). Histogram results also tell us which wavelet suits best for studying well-log data. Accordingly, Fig. 8 and Tables 1–4 clearly suggest that all four wavelets appear to be suitable for studying resistivity log data. Morlet and Sym2 wavelets do not appear to be suitable for studying gamma-ray, neutron porosity and velocity log data. Although the histograms of CWT coefficients of the Gaus3 wavelet suggest that it can be used to study all the logs, the resolution of subsurface formations in the scalogram plots due to this wavelet is less distinct compared to that of the Gaus1 wavelet. Therefore, based on the data used in the present study we conclude that the optimum wavelet identified for analysis of well log-data is the Gaus1 wavelet.

## 6 Conclusions

CWT is an efficient mathematical tool to analyze nonstationary signals like well-logs. Among the variety of wavelets used, we find that the Gaus1 wavelet shows good resolution in clearly delineating the boundaries of alternating sequences of shaly and nonshaly formations in different well-logs, considered in the present study, corresponding to three wells in the Bombay offshore basin, India. Compared to that of the Gaus1 wavelet, the depth resolution of formations in the scalogram plots of Gaus3 wavelet corresponding to all the three wells is less distinct. Use of Morlet and Sym2



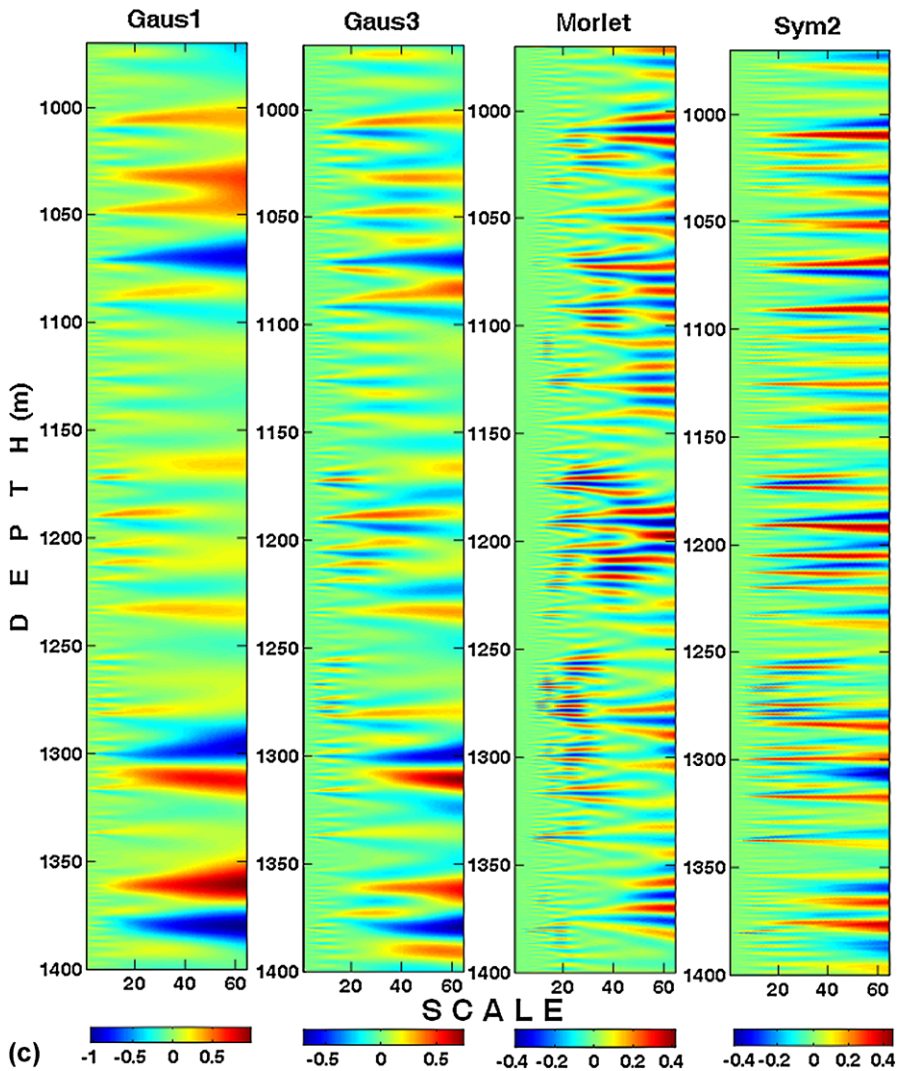


Fig. 7 (Continued)

wavelets in the analyses of gamma-ray, neutron porosity, and velocity logs has not provided any useful information on the depth locations of formation boundaries in all three wells. Histogram analysis of the CWT coefficients also supports these observations (Fig. 8) and thus becomes important in the kind of studies described here. Depths to the tops of the formation zones could be clearly demarcated in the CWT analysis of the gamma-ray log (with Gaus1 and Guas3 wavelets) and resistivity log (with all four wavelets) data. The calculated estimates of the depths to the tops of the L-I, L-II, S-I, and L-III formations obtained from the scalogram plots of Gaus1 and Gaus3 wavelets, corresponding to different log data sets of all the wells match well with the known information on the depths of these formations in the study area.

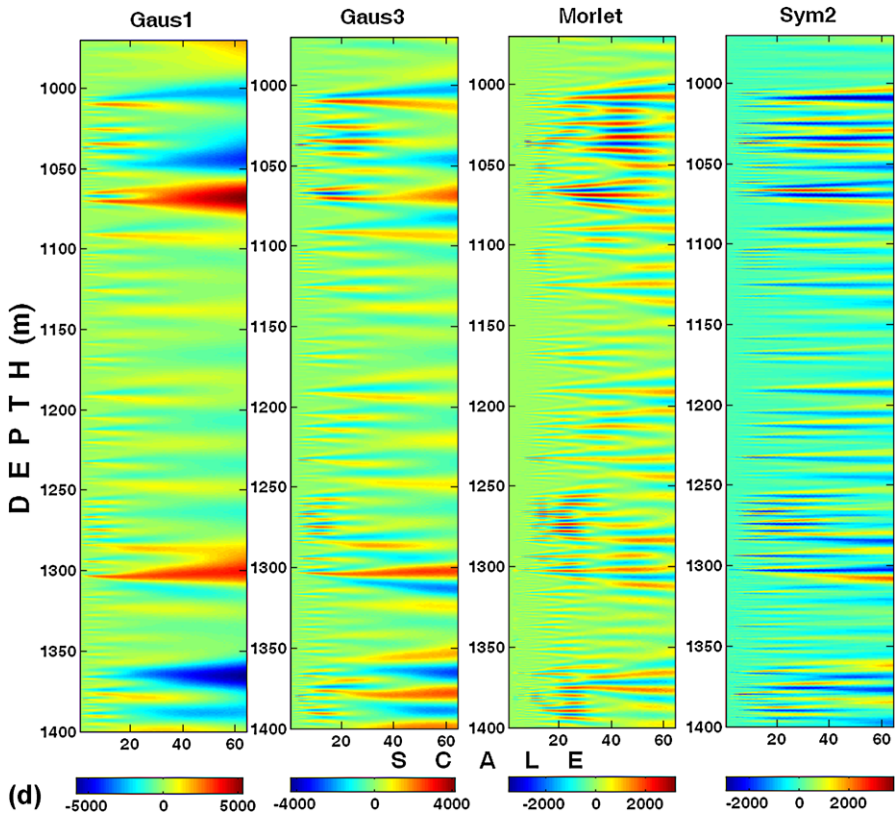


Fig. 7 (Continued)

Analysis of further data sets from wells in other regions is largely worthwhile and necessary in order to globally optimize whether or not the Gaus1 wavelet can be proclaimed to be the most suitable wavelet for analyzing well-log data.

**Acknowledgements** The authors thank ONGC Ltd., India, for providing us with the data and for their permission to publish this work. EC thanks V.M. Gadre for helpful discussions on the mathematical details given in Appendix C. He also thanks Santanu Banerjee for useful discussions on the geology and lithostratigraphic details of the study area. The authors thank the editor and two anonymous referees for their meticulous reviews, which have improved the quality of the paper.

**Appendix A**

Let  $f_{\delta x}(x) = f(x - \delta x)$  be the spatial shift in  $f(x) \in L^2(\mathbb{R})$  by a small amount,  $\delta x$ . The CWT of  $f_{\delta x}(x)$  is

$$\begin{aligned} \text{CWT}(f_{\delta x}(d, s)) &= \frac{1}{\sqrt{s}} \int_{-\infty}^{\infty} f(x - \delta x) \psi\left(\frac{x - d}{s}\right) dx \\ &= \frac{1}{\sqrt{s}} \int_{-\infty}^{\infty} f(x') \psi\left(\frac{x' - (d - \delta x)}{s}\right) dx \quad \text{where } x' = x - \delta x \\ &= \text{CWT}(f(d - \delta x, s)). \end{aligned}$$

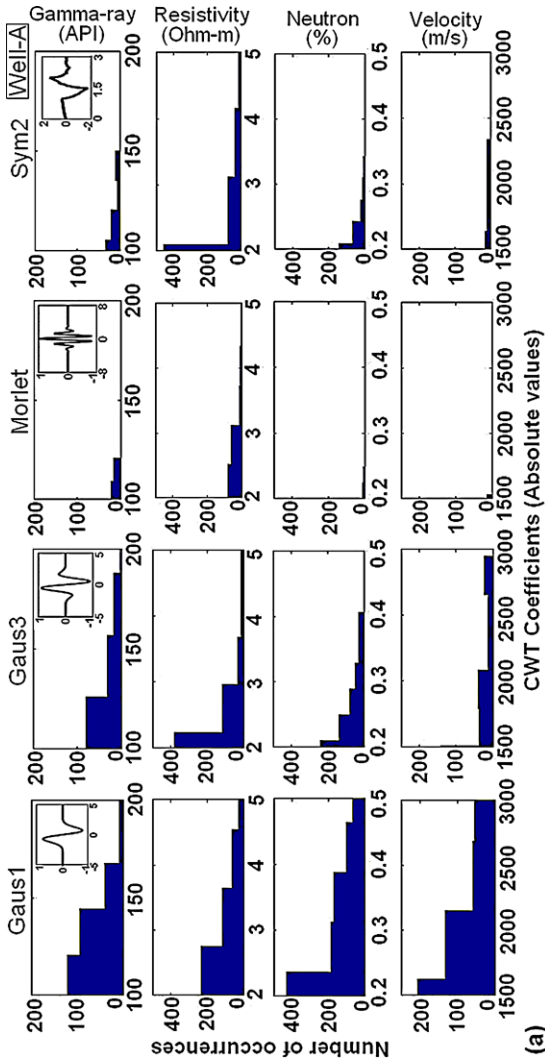


**Fig. 8** Histogram analysis results of Gaus1, Gaus3, Morlet, and Sym2 wavelets corresponding to (a) Well-A, (b) Well-B, and (c) Well-C. The number of occurrences designates the number of times a CWT coefficient occurred. Insets show the shapes of respective wavelets

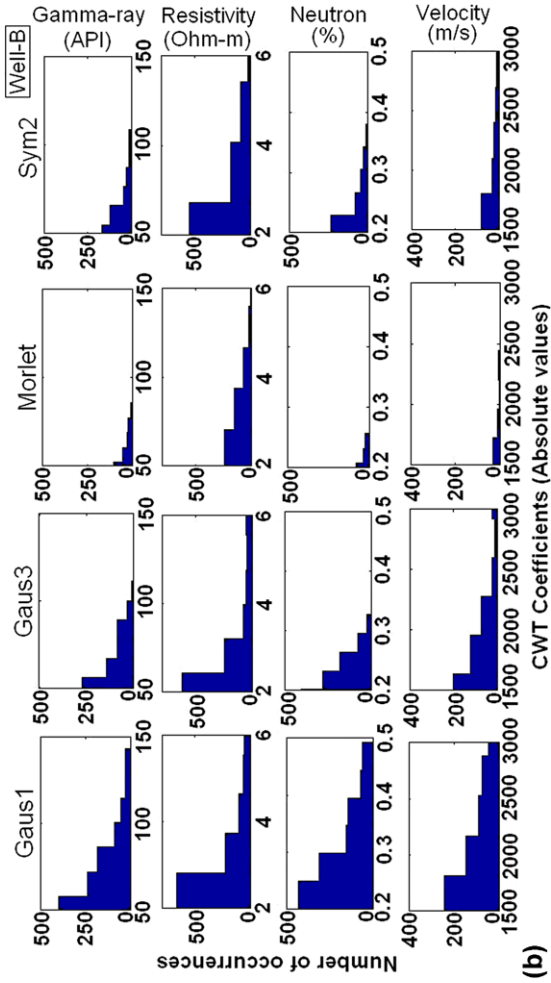


Fig. 8 (Continued)

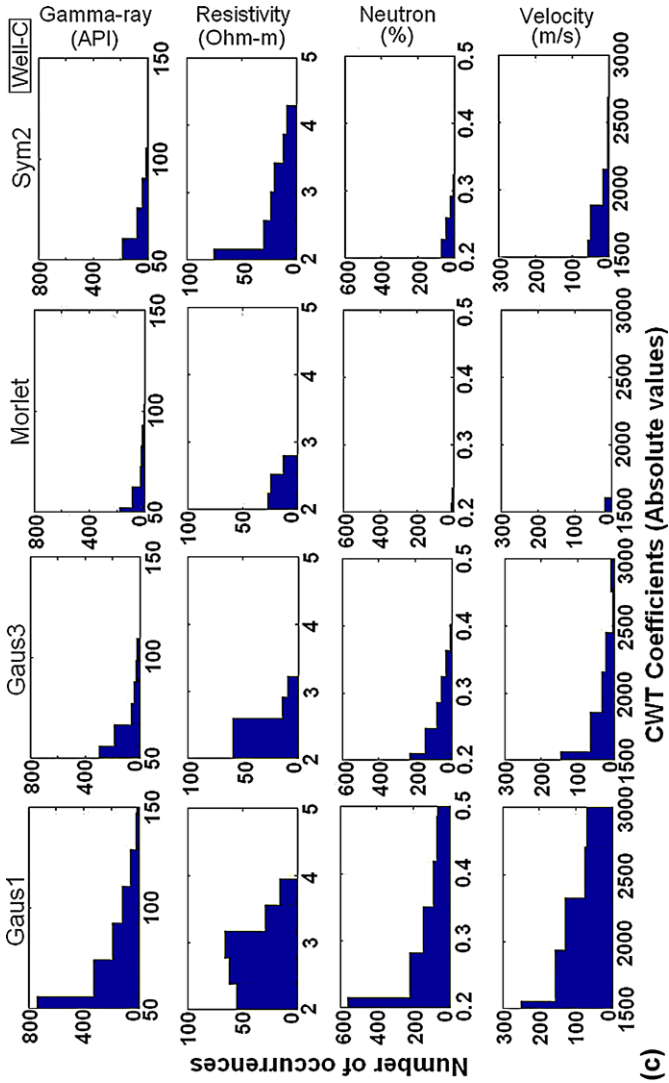


Fig. 8 (Continued)

**Table 1** Comparison of the estimated depths of formation tops from the scalogram plots of Gaus1 wavelet for different well-logs with the known depth estimates provided by ONGC Ltd. Note the good agreement between the observed and estimated values

Gaus1	Formations	Known depths provided by ONGC Ltd. (in m)	Gamma-ray	Resistivity	Neutron porosity	Velocity
Well-A	L-I	998.5	998	998	997	997.6
	L-II	1020	1021	1022	1022	1021
	S-I	1226	1225	1225	1225	1226
	L-III	1350	1352	1351	1351	1352
Well-B	L-I	980.5	983	980.5	980.2	984
	L-II	1006	1006	1000	1008	1007
	S-I	1202	1200	1201	1201	1201
	L-III	1329	1329	1329	1328	1331
Well-C	L-I	1004	1003	1003	1004	1004
	L-II	1032	1031	1032	1032	1033
	S-I	1195	1200	1200	1189	Not clear
	L-III	1361	1361	1361	1361	1361

**Table 2** Same as Table 1, but for Gaus3 wavelet

Gaus3	Formations	Known depths provided by ONGC Ltd. (in m)	Gamma-ray	Resistivity	Neutron porosity	Velocity
Well-A	L-I	998.5	998	998	996	995
	L-II	1020	1021	1021	1021	1021
	S-I	1226	1223	1226	1226	1227
	L-III	1350	1351	1356	1351	1350
Well-B	L-I	980.5	980	981	979	983
	L-II	1006	1005	1009	1005	1007
	S-I	1202	1205	1220	1198	Not clear
	L-III	1329	1326	1329	1326	1328
Well-C	L-I	1004	1004	1004	1004	1004
	L-II	1032	1031	1033	1032	1030
	S-I	1195	1201	1199	1187	1190
	L-III	1361	1361	1360	1361	1364

Since the output is shifted the same way as the input signal, the CWT is shift-invariant. Similarly, the shift-invariant property for DWT, where the shifts are in dyadic scales also can be shown. For further details, the reader is referred to Ma and Tang (2001).

**Table 3** Same as Table 1, but for Morlet wavelet

Morlet	Formations	Known depths provided by ONGC Ltd. (in m)	Gamma-ray	Resistivity	Neutron porosity	Velocity
Well-A	L-I	998.5	Not clear	996	997	997
	L-II	1020	Not clear	1022	Not clear	1023
	S-I	1226	Not clear	Not clear	1223	Not clear
	L-III	1350	1348	1353	Not clear	1352
Well-B	L-I	980.5	Not clear	980	Not clear	983
	L-II	1006	Not clear	Not clear	Not clear	Not clear
	S-I	1202	1206	Not clear	1200	Not clear
	L-III	1329	1329	1329	Not clear	1327
Well-C	L-I	1004	Not clear	1004	1005	1005
	L-II	1032	1030	1033	Not clear	Not clear
	S-I	1195	1193	1200	1194	1194
	L-III	1361	1361	1360	Not clear	Not clear

**Table 4** Same as Table 1, but for Sym2 wavelet

Sym2	Formations	Known depths provided by ONGC Ltd. (in m)	Gamma-ray	Resistivity	Neutron porosity	Velocity
Well-A	L-I	998.5	Not clear	997	995	1000
	L-II	1020	Not clear	1022	Not clear	1019
	S-I	1226	Not clear	1225	1225	Not clear
	L-III	1350	1350	1351	Not clear	1351
Well-B	L-I	980.5	Not clear	980	983	Not clear
	L-II	1006	1004	1005	Not clear	1005
	S-I	1202	1206	1220	Not clear	Not clear
	L-III	1329	1328	1329	Not clear	Not clear
Well-C	L-I	1004	Not clear	1004	1004	1004
	L-II	1032	Not clear	1031	Not clear	Not clear
	S-I	1195	1201	1199	1199	Not clear
	L-III	1361	1359	1358	Not clear	1361

## Appendix B

The following provides a brief guide of the mathematical representations of the wavelets used in the present study:

### 1. Gaussian wavelets

The Gaussian wavelet of  $n$ th order is defined as

$$\psi_n(x) = C_n f^{(n)}(x), \quad (\text{B.1})$$

where  $f^{(n)}(x)$  denotes the  $n$ th derivative of the Gaussian function and  $f(x) = \exp(-x^2)$ . Here,  $C_n$  is such that  $\|f^{(n)}(x)\|^2 = 1$ . Considering  $n = 1$  and  $3$  in (B.1), we get Gaus1 and Gaus3 wavelets, respectively.

**2. Morlet wavelet**

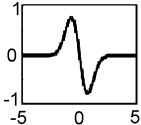
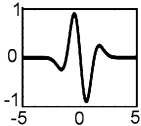
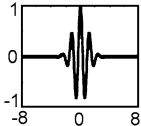
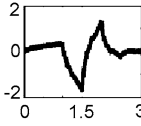
Morlet wavelet is obtained by multiplying the complex exponential function with the Gaussian function. As a result, Morlet wavelet is a complex wavelet. Since only the real wavelet is used in the present study, the real valued Morlet wavelet is usually defined as

$$\psi(x) = \frac{1}{\sqrt[4]{\pi}} \exp(-x^2) \cos(\omega_0 x) \quad \omega_0 \geq 5. \tag{B.2}$$

The wavelet function,  $\psi(x)$  satisfies the admissibility condition only when  $\omega_0 \geq 5$  (Kumar and Foufoula-Georgiou 1994).

**3. Symlet wavelet**

Symlets are also known as Daubechies’ least-asymmetric wavelets. They are near symmetric, and like Daubechies’ wavelets, are also orthogonal. They are compactly supported and have finite vanishing moments. For more details of the Symlet family of wavelets, the reader is referred to Daubechies (1992):

Name of the wavelet	Shape of the wavelet*	Symmetry	Compact support	Orthogonality	Vanishing moments
Gaus1		Anti-symmetric	No	No	Arbitrary
Gaus3		Anti-symmetric	No	No	Arbitrary
Morlet		Symmetric	No	No	Arbitrary
Sym2		Near symmetric	Yes	Yes	2

\*The horizontal and vertical axes for the wavelet shapes are in arbitrary units.

**Symmetry:** The symmetry property of wavelets explains that the wavelet transform (WT) of the mirror (m) of a signal is mirror of the wavelet transform of the signal. That is,  $WT\{m[f(t)]\} = m\{WT[f(t)]\}$ .



*Compact support:* This property explains that the wavelet vanishes outside a finite interval. Shorter intervals indicate higher compactness of the wavelet.

*Orthogonality:* This property implies that if it is possible to construct some wavelets  $\psi(t)$ , such that  $\psi_{u,v}(t)$  are orthonormal. That is,  $\int \psi_{u,v}(t)\psi_{u',v'}(t) dt = \delta_{uu'}\delta_{vv'}$ , where  $\delta_{i,j}$  denotes the delta function, then such wavelets are orthogonal to their translations and dilations.

*Vanishing moments:* A wavelet,  $\psi(t)$  has  $N$  vanishing moments, if the Fourier transform of the wavelet at the origin, is  $k$  times continuously differentiable. That is,  $\frac{d^k}{d\omega^k} \psi(\omega = 0) = 0$ , for  $k = 0, 1, \dots, N - 1$ . In other words, if a wavelet has  $N$  vanishing moments, then wavelet-coefficients for  $N$ th order polynomial corresponding to that wavelet will be zero. This implies that any polynomial signal up to order  $N - 1$  can be represented completely in scaling space. In theory, if a wavelet has more vanishing moments, its scaling function can represent more complex signals accurately.  $N$  is also called the accuracy of the wavelet. For more details, the reader is referred to Strang and Nguyen (1995).

### Appendix C

Let a signal,  $x(t)$ , centered at origin, be finite and square integrable; that is,  $x(t) \in L^2(\mathbb{R})$ , which can be written as

$$\int_{-\infty}^{\infty} |x(t)|^2 dt = \|x\|_2^2. \tag{C.1}$$

The probability density function (PDF) of  $x(t)$  in time and frequency domains can be written as

$$P_x(t) = \frac{|x(t)|^2}{\|x\|^2} \quad \text{and} \quad P_x(\omega) = \frac{|x(\omega)|^2}{\|x\|^2}.$$

The variance of each of these is a measure of corresponding uncertainties. Accordingly, for zero-mean signals, both in time and frequency, we have

$$\sigma_t^2 = \frac{\int_{-\infty}^{\infty} t^2 |x(t)|^2 dt}{\|x\|_2^2} \quad \text{and} \quad \sigma_\omega^2 = \frac{\int_{-\infty}^{\infty} \omega^2 |x(\omega)|^2 d\omega}{\|x\|_2^2}. \tag{C.2}$$

From the differentiation property of Fourier transformation,  $\sigma_\omega^2$  can be written as

$$\sigma_\omega^2 = \frac{\int_{-\infty}^{\infty} \left| \frac{dx(t)}{dt} \right|^2 dt}{\|x\|_2^2}.$$

The product of time–frequency variance, also known as time bandwidth product (for a review, see Gadre 2011) is

$$\sigma_t^2 \sigma_\omega^2 = \frac{\int_{-\infty}^{\infty} t^2 |x(t)|^2 dt \int_{-\infty}^{\infty} \left| \frac{dx(t)}{dt} \right|^2 dt}{\|x\|_2^4}. \tag{C.3}$$

Using Eq. (C.1), Eq. (C.3) can be written as

$$\sigma_t^2 \sigma_\omega^2 = \frac{\|tx(t)\|_2^2 \left\| \frac{dx(t)}{dt} \right\|_2^2}{\|x\|_2^4}. \tag{C.4}$$

Equation (C.4) represents the uncertainty that lies in the simultaneous measurement of time and frequency. Now the problem is to find out how minimum this uncertainty is.

Let us consider two vectors  $\vec{v}_1$  and  $\vec{v}_2$ . According to the Cauchy–Schwarz inequality, their inner product for higher order terms is given by

$$\begin{aligned} |\langle \vec{v}_1, \vec{v}_2 \rangle|^2 &= |\vec{v}_1|^2 |\vec{v}_2|^2 \cos^2 \theta \quad (0 \leq \cos^2 \theta \leq 1) \\ \Rightarrow |\langle \vec{v}_1, \vec{v}_2 \rangle|^2 &\leq |\vec{v}_1|^2 |\vec{v}_2|^2. \end{aligned} \tag{C.5}$$

Consequently, the numerator of Eq. (C.4) can be written as

$$\begin{aligned} \|tx(t)\|_2^2 \left\| \frac{dx(t)}{dt} \right\|_2^2 &\geq \left| \left\langle tx(t), \frac{dx(t)}{dt} \right\rangle \right|^2 \\ &\geq \left| \int_{-\infty}^{\infty} tx(t) \frac{\overline{dx(t)}}{dt} dt \right|^2 \\ &\geq \left| \int_{-\infty}^{\infty} t \operatorname{Re} \left[ x(t) \frac{\overline{dx(t)}}{dt} \right] dt \right|^2, \end{aligned} \tag{C.6}$$

where,  $\frac{\overline{dx(t)}}{dt}$  indicates the complex conjugate of  $\frac{dx(t)}{dt}$  (as these expressions are also valid for complex functions). The real part of a complex function ( $z$ ) can be written as  $\operatorname{Re}(z) = (\frac{z+\bar{z}}{2})$ , where  $z = x(t) \frac{dx(t)}{dt}$  and its complex conjugate,  $\bar{z} = x(t) \frac{\overline{dx(t)}}{dt} = \overline{x(t) \frac{dx(t)}{dt}}$ . Thus,

$$\begin{aligned} \operatorname{Re} \left[ x(t) \frac{\overline{dx(t)}}{dt} \right] &= \frac{1}{2} \left[ x(t) \frac{\overline{dx(t)}}{dt} + \overline{x(t) \frac{dx(t)}{dt}} \right] \\ &= \frac{1}{2} \frac{d}{dt} [x(t) \cdot \overline{x(t)}] \\ &= \frac{1}{2} \frac{d}{dt} |x(t)|^2. \end{aligned}$$

Therefore, from Eq. (C.6), we have

$$\|tx(t)\|_2^2 \left\| \frac{dx(t)}{dt} \right\|_2^2 \geq \left| \frac{1}{2} \int_{-\infty}^{\infty} t \frac{d}{dt} |x(t)|^2 dt \right|^2. \tag{C.7}$$

Solving the integral in Eq. (C.7) using integration by parts, we get  $t|x(t)|^2|_{-\infty}^{\infty} - \int_{-\infty}^{\infty} |x(t)|^2 dt$ .

Since  $\int_{-\infty}^{\infty} t^2|x(t)|^2 dt$  is finite, and for the integral in Eq. (C.6) to converge,  $t|x(t)|^2|_{-\infty}^{\infty} = 0$  as  $t \rightarrow \pm\infty$ .

Accordingly, we have

$$\begin{aligned} \left\| tx(t) \right\|_2^2 \left\| \frac{dx(t)}{dt} \right\|_2^2 &\geq \frac{1}{4} \left| - \int_{-\infty}^{\infty} |x(t)|^2 dt \right|^2 \\ &\geq \frac{1}{4} \|x\|_2^4. \end{aligned}$$

Substituting the above value in Eq. (C.4), we get

$$\begin{aligned} \sigma_t^2 \sigma_\omega^2 &\geq \frac{\frac{1}{4} \|x\|_2^4}{\|x\|_2^4} \\ \sigma_t^2 \sigma_\omega^2 &\geq \frac{1}{4} = 0.25. \end{aligned}$$

This proves that the uncertainty in the measurement of any two parameters such as time–frequency or position–momentum, etc., can never be less than 0.25. The equality in Eq. (C.5) can be achieved, only when  $\cos^2 \theta = 1$ . This implies that the two vectors  $[\vec{v}_1 = tx(t)]$  and  $[\vec{v}_2 = \frac{dx(t)}{dt}]$  must be collinear (that is, linearly dependent). This leads to

$$\frac{dx(t)}{dt} = A_0 tx(t) \quad (A_0 = \text{constant}). \quad (\text{C.8})$$

Equation (C.8) can be solved to get  $x(t) = Ce^{A_0 t^2/2}$ . Since the functions we considered are finite,  $A_0$  must be a negative real number (say,  $-1$ ) and  $C$  is a constant. Therefore, the optimal analyzing function, which enables time-frequency representation of a signal with least uncertainty is the Gaussian function,  $x(t) = e^{-t^2/2}$ . The same analogy can be extended to space-domain signals like well-logs.

## References

- Anxionnaz H, Delfiner P, Delhomme JP (1990) Computer-generated core-like descriptions from open-hole logs. *Am Assoc Pet Geol Bull* 74:375–393
- Bhandari LL, Jain SK (1984) Reservoir geology and its role in the development of the L-III reservoir, Bombay high field. *Indian J Pet Geol* 7:27–46
- Biswas SK (1982) Rift basins in western margin of India and their hydrocarbon prospects with special reference to Kutch Basin. *Am Assoc Pet Geol Bull* 66:1497–1513
- Choudhury S, Chandrasekhar E, Pandey VK, Prasad M (2007) Use of wavelet transformation for geophysical well-log data analysis. *IEEE Xplore*. doi:10.1109/ICDSP.2007.4288665
- Daubechies I (1992) Ten lectures on wavelets. SIAM, Philadelphia
- Gadre VM (2011) Wavelets and multirate digital signal processing: time–bandwidth product. Video lecture, Dept. of Electrical Engineering, IIT, Bombay. URL. <http://www.youtube.com/watch?v=zYVW6ENk9w>
- Jansen FE, Kelkar M (1997) Application of wavelets to production data in describing inter-well relationships. In: *Soc Petr Engr # 38876: annual technical conference and exhibition*. San Antonio, TX, October 5–8, 1997
- Jennings JW, Ruppel SC, Ward WB (2000) Geostatistical analysis of permeability data and modeling of fluid-flow effects in carbonate outcrops. *SPE Reserv Eval* 3:292–303
- Kumar P, Foufoula-Georgiou E (1994) Wavelet analysis in geophysics: an introduction. In: Foufoula-Georgiou E, Kumar P (eds) *Wavelets in geophysics*. Academic Press, San Diego, pp 1–43
- Ma K, Tang X (2001) Translation-invariant face feature estimation using discrete wavelet transform. In: Tang YY, et al (eds) *Proceedings of the second international conference on wavelet analysis and its applications*. LNCS, vol 2251. Springer, Berlin, Heidelberg, pp 200–210

- Mallat S (1989) A theory for multiresolution signal decomposition: the wavelet representation. *IEEE Trans Pattern Anal Mach Intell* 11:674–693
- Mallat S (1999) A wavelet tour of signal processing, 2nd edn. Academic Press, San Diego
- Panda MN, Mosher CC, Chopra AK (2000) Application of wavelet transforms to reservoir—data analysis and scaling. *SPE J* 5:92–101
- Prokoph A, Agterberg FP (2000) Wavelet analysis of well-logging data from oil source rock, Egret Member offshore eastern Canada. *Am Assoc Pet Geol Bull* 84:1617–1632
- Rao PR, Srivastava DC (1981) Seismic stratigraphy of western Indian offshore. In: Geological interpretation of geophysical data, IPE. ONGC Ltd., India, pp 49–57
- Rivera N, Ray S, Chan AK, Jensen J (2002) Well-log feature extraction using wavelets and genetic algorithms. In: Proc Am Assoc Petr Geol ann meeting, Houston, Texas, 10–13 March, 2002
- Rivera N, Ray S, Chan AK, Ayers WB (2004) Detection of cyclic patterns using wavelets: an example study in the Ormskirk sandstone. *Irish Sea Math Geol* 36:529–543
- Serra O, Abbot HT (1982) The contribution of logging data to sedimentology and stratigraphy. *SPE J* 22 (February):117–135
- Soliman MY, Ansah J, Stephenson S, Manda B (2001) Application of wavelet transform to analysis of pressure transient data. In: Soc Petr Engr # 71571: SPE annual technical conference and exhibition, New Orleans, 30 September–3 October 2001
- Strang G, Nguyen T (1995) Wavelets and filter banks. Wellesley–Cambridge Press, Prentice Hall
- Tiwari RK (1987) Higher order eccentricity cycles of the late and mid Miocene climatic variations. *Nature* 327:219–221
- Vega NR (2003) Reservoir characterization using wavelet transforms. PhD dissertation, Texas A&M University, USA
- Wolff M, Pelissier-Combesure J (1982) FACIOLOG: automatic electrofacies determination. In: Society of Professional well log analysts annual logging symposium, 6–9, paper FF